JOURNAL OF GUIDANCE, CONTROL, AND DYNAMICS
Vol. 21, No. 4, July–August 1998

Analytical Criterion for Chaotic Dynamics in Flexible Satellites with Nonlinear Controller Damping

Gary L. Gray*
Pennsylvania State University, University Park, Pennsylvania 16802
Andre P. Mazzoleni†
Texas Christian University, Fort Worth, Texas 76129
and
David R. Campbell III‡
Lockheed Martin Manned Space Systems, New Orleans, Louisiana 70189

In this work, we study the attitude dynamics of a single body spacecraft that is perturbed by the motion of a small flexible appendage constrained to undergo only torsional vibration. In particular, we are interested in the chaotic dynamics that can occur for certain sets of the physical parameter values of the spacecraft when energy dissipation acts to drive the body from minor to major axis spin. Energy dissipation, which is present in all spacecraft systems and is the mechanism that drives the minor to major axis transition, is implemented by a quantitative energy sink that is modeled with a nonlinear controller. We obtain an analytical test for chaos in terms of satellite parameters by Melnikov's method. This analytical criterion provides a useful design tool to spacecraft engineers who are concerned with avoiding potentially problematic chaotic dynamics in their systems. In addition, we show that a spacecraft with a control system designed to provide energy dissipation can exhibit chaos because of the inherent flexibility of its components.

Introduction

THIS paper deals with the attitude dynamics of a single body spacecraft with a small flexible appendage whose motion is limited to torsional vibration.[1–3] In addition, energy dissipation is introduced by use of a nonlinear controller defined by Kammer and Gray.[4] The nonlinear controller quantitatively simulates an energy sink that dissipates energy from the system without adding additional degrees of freedom. We study the chaotic dynamics that can occur for certain sets of the physical parameter values of the spacecraft when energy dissipation acts to drive the body from minor to major axis spin. We obtain an analytical criterion for chaos in terms of physical parameters of the satellite.

This work is an extension of earlier work of Gray et al.,[5–7] in which chaotic attitude dynamics occurring in simple spacecraft system were analytically investigated. In Ref. 5, Melnikov's method[8–10] is used to investigate the onset of chaotic dynamics in a viscously damped spacecraft that has small subbodies oscillating within it. In Ref. 6, the same model is studied as in Ref. 5, but damping is implemented via the nonlinear controller used in this paper. In Ref. 7, Gray and Campbell numerically investigate the dynamics of the model used in Ref. 5, and in doing so develop numerical tools for studying chaos in spacecraft systems, demonstrating the richness of dynamics that are possible in simple spacecraft systems.

Other related work includes the analytical study of chaos in Hamiltonian[11] spacecraft models that possess a rotor aligned with a principal axis by Holmes and Marsden,[12] a Hamiltonian dual-spin spacecraft model by Koiller,[13] perturbation studies of spacecraft with elastic and dissipative elements by Chernous'ko,[14,15] and the analytical and numerical study by Kaplan et al.[16,17] of the use of the apogee motor with paired satellites technique to deploy pairs of satellites into high circular orbits. Excellent reviews of some of this work and much more can be found.[18,19]

This work differs from previous studies in that we are able to analytically predict chaotic dynamics in non-Hamiltonian spacecraft models. In addition, we are able to predict global dynamics, i.e., necessary conditions for chaotic attitude dynamics, in terms of the system parameters. Finally, unlike the earlier analytical work of Gray et al., continuous elastic elements are present, which results in a substantial complication of the equations of motion and the analysis. It is important to note that we study chaotic dynamics in a spacecraft system with energy dissipation that does not possess nonautonomous forcing terms. In other words, the chaos comes from the vibration of continuous elastic elements on the spacecraft and not from some nonautonomous periodic forcing function such as a misaligned rotor. Thus, we show that even a perfectly tuned spacecraft system, with a control system designed to provide energy dissipation, can exhibit chaos because of the inherent flexibility of its components.

Problem Description

The model system shown in Fig. 1 consists of a torque-free, undamped, rigid carrier body b that is perturbed by two effects: the motion of an elastic appendage a cantilevered off carrier body b and an onboard nonlinear controller that quantitatively simulates an energy sink.[4]

In addition, we impose the following conditions on the system: Appendage a consists of a rigid tip mass that is joined to carrier body b by a massless elastic rod. The mass center of the entire spacecraft, or rather the system, is located at $\mathcal{CM}$ and that of the appendage is at $\mathcal{CM}_a$. The orthonormal coordinate system, e_1, e_2, e_3, affixed to the carrier body and originating at the system's mass center $\mathcal{CM}$, is parallel to the appendage's orthonormal coordinate system ζ_1, ζ_2, ζ_3, which originates at its mass center $\mathcal{CM}_a$. Both sets of basis vectors are body-fixed with respect to carrier body b. The distance between the two mass centers along the coincident unit vectors $\hat{e}_1$, $\hat{\zeta}_1$ is ℓ. (Throughout this work, we denote a unit vector in the direction q by $\hat{q}$.) The mass moment of inertia tensors of appendage a and carrier body b are denoted $\mathrm{diag}\{A_a, B_a, C_a\}$ and $\mathrm{diag}\{A_b, B_b, C_b\}$, respectively, with $A_b < B_b < C_b$. The previous inequalities must be strict in the sense that the carrier body must be asymmetric. This assumption is not needed for derivation of the equations of motion but will be needed for application of Melnikov's method. The components of the inertial angular velocity of carrier

Received Aug. 7, 1996; revision received June 16, 1997; accepted for publication June 23, 1997.

*Assistant Professor, Department of Engineering Science and Mechanics, 227 Hammond Building. E-mail: glgesm@engr.psu.edu. Member AIAA.
†Associate Professor, Department of Engineering. E-mail: a.mazzoleni@tcu.edu. Senior Member AIAA.
‡Senior Load and Dynamics Engineer, Michoud Assembly Facility, 13800 Old Gentilly Road.

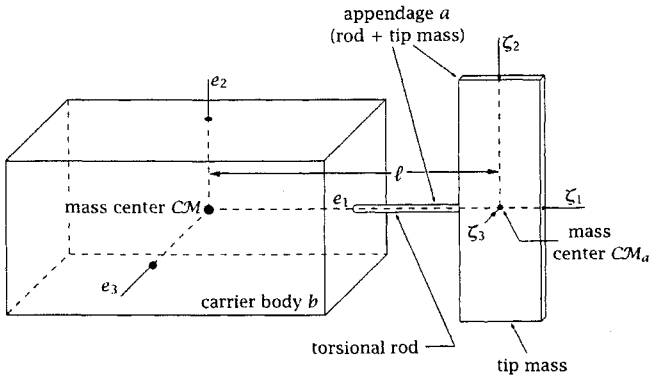

Fig. 1 Spacecraft model.

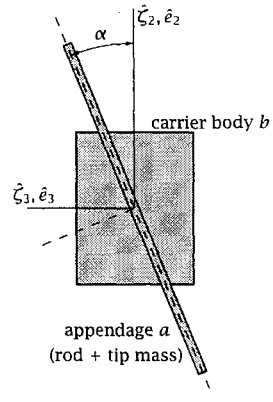

Fig. 2 Profile view of spacecraft model in deformed state.

body b, ω, are defined by the expression $\omega = \omega_1\hat{e}_1 + \omega_2\hat{e}_2 + \omega_3\hat{e}_3$. The motion of the tip mass (see Fig. 2) is limited to rotation about the rod axis, e_1 or ζ_1. This torsional displacement mode can be realized if the appendage is constrained by a system of guy wires that prevent flexural and flexural-torsional vibration modes.[1–3] Consequently, the system's mass center does not move relative to carrier body b. The angle of twist of the torsional elastic rod relative to the carrier body is measured by angle α. The rod extends from the outer surface of the carrier body to the origin of the ζ_1, ζ_2, ζ_3 coordinate system and has a torsional stiffness of JG/L. The cross section of the rod is circular. The system is free of any external torques or forces that might stem from gravity gradients, atmospheric drag, thermal gradients, or the like. The control gain of the nonlinear controller is measured by the parameter β and is incorporated into the equations of motion according to Kammer and Gray.[4]

Equations of Motion

Now that the model has been defined, the equations of motion are derived for the carrier body by using standard Newton–Euler techniques. The procedure we undertake is as follows: The satellite's total angular momentum with respect to its mass center CM is given by

$$\begin{aligned}\boldsymbol{h}_{CM} &= [A_b\omega_1 + A_a(\omega_1 + \dot{\alpha})]\hat{e}_1 \\ &+ \left[B_b\omega_2 - \left(C_a + m_a\ell^2\right)(\omega_3\cos\alpha - \omega_2\sin\alpha)\sin\alpha\right. \\ &+ \left.\left(B_a + m_a\ell^2\right)(\omega_2\cos\alpha + \omega_3\sin\alpha)\cos\alpha\right]\hat{e}_2 \\ &+ \left[C_b\omega_3 + \left(C_a + m_a\ell^2\right)(\omega_3\cos\alpha - \omega_2\sin\alpha)\cos\alpha\right. \\ &+ \left.\left(B_a + m_a\ell^2\right)(\omega_2\cos\alpha + \omega_3\sin\alpha)\sin\alpha\right]\hat{e}_3 \end{aligned} \tag{1}$$

with the corresponding components

$$\boldsymbol{h}_{CM} = h_1\hat{e}_1 + h_2\hat{e}_2 + h_3\hat{e}_3 \tag{2}$$

It will be advantageous later if we equate the two forms of the total angular momentum given in Eqs. (1) and (2) now and then solve for the angular velocities ω_i in terms of the components of angular momentum h_i. Doing this, we obtain the following three equations:

$$\omega_1 = \frac{h_1 - A_a\dot{\alpha}}{A_b + A_a} \tag{3}$$

$$\begin{aligned}\omega_2 &= \left\{\tfrac{1}{2}h_2\left[B_a + C_a + 2C_b + 2m_a\ell^2 + (C_a - B_a)\cos 2\alpha\right]\right. \\ &- \left.\tfrac{1}{2}h_3(B_a - C_a)\sin 2\alpha\right\}\Big/\left[\tfrac{1}{2}(B_aB_b + B_bC_a + B_aC_b\right. \\ &+ \left.C_aC_b) + \tfrac{1}{2}(-B_aB_b + B_bC_a + B_aC_b - C_aC_b)\cos 2\alpha\right. \\ &+ \left.B_aC_a + B_bC_b + m_a\ell^2\left(B_a + B_b + C_a + C_b + m_a\ell^2\right)\right] \end{aligned} \tag{4}$$

$$\begin{aligned}\omega_3 &= \left\{\tfrac{1}{2}h_3\left[B_a + C_a + 2B_b + 2m_a\ell^2 - (C_a - B_a)\cos 2\alpha\right]\right. \\ &- \left.\tfrac{1}{2}h_2(B_a - C_a)\sin 2\alpha\right\}\Big/\left[\tfrac{1}{2}(B_aB_b + B_bC_a + B_aC_b\right. \\ &+ \left.C_aC_b) + \tfrac{1}{2}(-B_aB_b + B_bC_a + B_aC_b - C_aC_b)\cos 2\alpha\right. \\ &+ \left.B_aC_a + B_bC_b + m_a\ell^2\left(B_a + B_b + C_a + C_b + m_a\ell^2\right)\right] \end{aligned} \tag{5}$$

The equations of motion can now be determined by taking the total time derivative of the angular momentum and setting it equal to the sum of all external torques about the mass center CM, $\boldsymbol{M}_{CM}$. Expanding the total time derivative, we arrive at the relation

$$\boldsymbol{M}_{CM} = \frac{D\boldsymbol{h}_{CM}}{Dt} = \frac{\mathrm{d}\boldsymbol{h}_{CM}}{\mathrm{d}t} + \boldsymbol{\omega} \times \boldsymbol{h}_{CM} \tag{6}$$

where $\mathrm{d}\boldsymbol{h}_{CM}/\mathrm{d}t$ represents the time derivative of $\boldsymbol{h}_{CM}$ in the rotating reference frame.

As we have assumed the system to be torque free, Eq. (6) can be written in terms of its components as

$$\dot{h}_1 = \omega_3h_2 - \omega_2h_3 \tag{7}$$

$$\dot{h}_2 = \omega_1h_3 - \omega_3h_1 \tag{8}$$

$$\dot{h}_3 = \omega_2h_1 - \omega_1h_2 \tag{9}$$

where the angular velocity terms ω_i were found in Eqs. (3–5). These three equations of motion are thus given by

$$\begin{aligned}\dot{h}_1 &= \left\{2[B_b - C_b + (B_a - C_a)\cos 2\alpha]h_2h_3\right. \\ &+ \left.(B_a - C_a)\left(h_3^2 - h_2^2\right)\sin 2\alpha\right\}\Big/\left\{B_b(B_a + 2C_b + C_a)\right. \\ &+ B_a(C_b + 2C_a) + C_bC_a + 2m_a^2\ell^4 + 2m_a\ell^2(B_b + B_a \\ &+ \left.C_b + C_a) + (B_a - C_a)(C_b - B_b)\cos 2\alpha\right\} - \beta h_1h_2^2 \end{aligned} \tag{10}$$

$$\begin{aligned}\dot{h}_2 &= 2\left\{\left[2B_b + B_a + C_a + 2m_a\ell^2 + (B_a - C_a)\cos 2\alpha\right]h_1h_3\right. \\ &- \left.(B_a - C_a)h_1h_2\sin 2\alpha\right\}\Big/\left\{(B_a - C_a)^2\sin^2 2\alpha\right. \\ &- \left[2B_b + B_a + C_a + 2m_a\ell^2 + (B_a - C_a)\cos 2\alpha\right] \\ &\times \left.\left[2C_b + B_a + C_a + 2m_a\ell^2 + (C_a - B_a)\cos 2\alpha\right]\right\} \\ &+ \frac{(h_1 - A_a\dot{\alpha})h_3}{A_b + A_a} + \beta h_2\left(h_1^2 - h_3^2\right) \end{aligned} \tag{11}$$

$$\begin{aligned}\dot{h}_3 &= \left\{\left[2C_b + B_a + C_a + 2m_a\ell^2 + (C_a - B_a)\cos 2\alpha\right]h_1h_2\right. \\ &+ \left.(C_a - B_a)h_1h_3\sin 2\alpha\right\}\Big/\left[B_b(B_a + 2C_b + C_a)\right. \\ &+ B_a(C_b + 2C_a) + C_bC_a + 2m_a^2\ell^4 + 2m_a\ell^2(B_b + B_a \\ &+ \left.C_b + C_a) + (B_a - C_a)(C_b - B_b)\cos 2\alpha\right] \\ &- \frac{(h_1 - A_a\dot{\alpha})h_2}{A_b + A_a} + \beta h_2^2h_3 \end{aligned} \tag{12}$$

where we have included the term due to the nonlinear controller in each equation. We note that the values of β must be restricted by the following two inequalities (see Ref. 4 for details):

$$\beta < \frac{2}{h}\sqrt{\left(\frac{C_b - A_b}{A_b C_b}\right)\left|\frac{A_b - B_b}{A_b B_b}\right|}$$
$$\beta < \frac{2}{h}\sqrt{\left(\frac{C_b - A_b}{A_b C_b}\right)\left|\frac{B_b - C_b}{B_b C_b}\right|} \tag{13}$$

and h is the total angular momentum of the system.

The appendage equation of motion is found by forming the Lagrangian of the whole system and then retaining only those terms that are functions of the angle α or its time derivative $\dot{\alpha}$. This reduced Lagrangian is given by

$$\mathcal{L} = \tfrac{1}{2}A_a\left(\dot{\alpha}^2 + 2\dot{\alpha}\omega_1 + \omega_1^2\right) + \tfrac{1}{2}B_a(\omega_2\cos\alpha + \omega_3\sin\alpha)^2$$
$$+ \tfrac{1}{2}C_a(-\omega_2\sin\alpha + \omega_3\cos\alpha)^2 - (JG/2L)\alpha^2 \tag{14}$$

Our last equation of motion is then found by applying Lagrange's equation of motion, giving

$$\frac{A_b A_a}{A_b + A_a}\ddot{\alpha} + \frac{A_a}{A_b + A_a}\dot{h}_1 + (C_a - B_a)(\omega_2\cos\alpha + \omega_3\sin\alpha)$$
$$\times(\omega_3\cos\alpha - \omega_2\sin\alpha) + \frac{JG}{L}\alpha = Q_\alpha = 0 \tag{15}$$

where ω_2 and ω_3 were found in Eqs. (4) and (5), $\dot{h}_1$ from Eq. (10) does not include the nonlinear controller term,[4] and the generalized force Q_α is assumed to be zero.

Nondimensionalization of the Equations of Motion

Our next step is to nondimensionalize Eqs. (10–12) and (15) and then transform them into a form consisting of an unperturbed part (the equations for a torque-free rigid body, i.e., Euler's equations) plus perturbation terms, thus leading to a system of the form

$$\dot{\boldsymbol{x}} = \boldsymbol{f}(\boldsymbol{x};\mu) + \varepsilon\boldsymbol{g}(\boldsymbol{x}, t;\mu) \tag{16}$$

where $\boldsymbol{x} = (h_1, h_2, h_3, \alpha, \dot{\alpha})$ and μ is a vector of system parameters. Writing the equations as an unperturbed part plus perturbation terms is required for application of Melnikov's method. This is the most difficult part of the modeling process because proper, yet reasonable, assumptions must be made about the relative sizes of all the physical quantities so that when order ε terms are discarded we are left with a properly integrable system. After consulting the literature,[20] we have formulated a set of assumptions about the relative sizes of the physical parameters.

Proceeding with the nondimensionalization, we assume the following orderings:

$$m_a\ell^2 = \mathcal{O}(\varepsilon), \qquad A_a = \mathcal{O}(\varepsilon), \qquad B_a = \mathcal{O}(\varepsilon)$$
$$C_a = \mathcal{O}(\varepsilon), \qquad C_a - B_a = \mathcal{O}(\varepsilon^2), \qquad \beta = \mathcal{O}(\varepsilon) \tag{17}$$

and that all other quantities are $\mathcal{O}(1)$. Physically, these assumptions imply that the tip mass is nearly symmetric ($C_a \approx B_a$), that the appendage is small compared with the main body in terms of total mass and of mass moments of inertia, and that the control gain β is small. Given these physical restrictions, we quantitatively define the following dimensionless quantities:

$$\varepsilon \triangleq \frac{m_a\ell^2}{B_b}, \qquad \tau \triangleq \frac{ht}{B_b}, \qquad \tilde{h}_i \triangleq \frac{h_i}{h}, \qquad \tilde{K} \triangleq \frac{JGB_b}{Lh^2}$$
$$\tilde{\beta} \triangleq \frac{hB_b}{\varepsilon}\beta, \qquad r_1 \triangleq \frac{C_b}{B_b}, \qquad r_2 \triangleq \frac{A_b}{B_b} \tag{18}$$
$$r_4 \triangleq \frac{A_a}{B_a}, \qquad \tilde{\lambda} \triangleq \frac{B_a}{\varepsilon B_b}, \qquad \tilde{\delta} \triangleq \frac{C_a - B_a}{\varepsilon m_a\ell^2}$$

where τ is nondimensional time and all nondimensional quantities except ε, α, τ, r_1, r_2, and r_4 are denoted with a tilde. We denote differentiation with respect to nondimensional time τ by a prime, and note that this implies that $()' \triangleq B_b()/h$. It is important to note that the definitions of nondimensional quantities given in Eq. (18) do not change the ordering of the physical parameters or constants even though it may appear so. For example, $\tilde{\lambda}$ is not an $\mathcal{O}(1/\varepsilon)$ quantity as it might first appear because B_a is $\mathcal{O}(\varepsilon)$.

Applying the nondimensional definitions, given in Eq. (18), to our equations of motion [Eqs. (10–12) and (15)], they are transformed into the following form:

$$\tilde{h}_1' = \left[2\left(1 - r_1 - \varepsilon^2\tilde{\delta}\cos 2\alpha\right)\tilde{h}_2\tilde{h}_3\right.$$
$$- \varepsilon^2\tilde{\delta}\sin 2\alpha\left(\tilde{h}_3^2 - \tilde{h}_2^2\right)\Big]\Big/\left\{2r_1 + 2\varepsilon(1 + r_1)(1 + \tilde{\lambda})\right.$$
$$+ \varepsilon^2[2 + \tilde{\delta}(1 + r_1) + 2\tilde{\lambda}(2 + \tilde{\lambda}) + \tilde{\delta}(1 - r_1)\cos 2\alpha]$$
$$\left. + 2\varepsilon^3\tilde{\delta}(1 + \tilde{\lambda})\right\} - \varepsilon\tilde{\beta}\tilde{h}_1\tilde{h}_2^2 \tag{19}$$

$$\tilde{h}_2' = 2\Big\{[2 + 2\varepsilon(1 + \tilde{\lambda}) + \varepsilon^2\tilde{\delta}(1 - \cos 2\alpha)]\tilde{h}_1\tilde{h}_3$$
$$+ \varepsilon^2(\tilde{\delta}\sin 2\alpha)\tilde{h}_1\tilde{h}_2\Big\}\Big/\Big\{\varepsilon^4\tilde{\delta}^2\sin^2 2\alpha - [2 + 2\varepsilon(1 + \tilde{\lambda})$$
$$+ \varepsilon^2\tilde{\delta}(1 - \cos 2\alpha)]\left[2r_1 + 2\varepsilon(1 + \tilde{\lambda}) + \varepsilon^2\tilde{\delta}(1 + \cos 2\alpha)\right]\Big\}$$
$$+ \varepsilon\tilde{\beta}\tilde{h}_2\left(\tilde{h}_1^2 - \tilde{h}_3^2\right) + \frac{(\tilde{h}_1 - \varepsilon\tilde{\lambda}r_4\alpha')\tilde{h}_3}{r_2 + \varepsilon\tilde{\lambda}r_4} \tag{20}$$

$$\tilde{h}_3' = \Big\{\left[2r_1 + 2\varepsilon(1 + \tilde{\lambda}) + \varepsilon^2\tilde{\delta}(1 + \cos 2\alpha)\right]\tilde{h}_1\tilde{h}_2$$
$$+ \varepsilon^2(\tilde{\delta}\sin 2\alpha)\tilde{h}_1\tilde{h}_3\Big\}\Big/\Big\{2r_1 + 2\varepsilon(1 + r_1)(1 + \tilde{\lambda})$$
$$+ \varepsilon^2[2 + \tilde{\delta}(1 + r_1) + 2\tilde{\lambda}(2 + \tilde{\lambda}) + \tilde{\delta}(1 - r_1)\cos 2\alpha]$$
$$+ 2\varepsilon^3\tilde{\delta}(1 + \tilde{\lambda})\Big\} + \varepsilon\tilde{\beta}\tilde{h}_2^2\tilde{h}_3 - \frac{(\tilde{h}_1 - \varepsilon\tilde{\lambda}r_4\alpha')\tilde{h}_2}{r_2 + \varepsilon\tilde{\lambda}r_4} \tag{21}$$

$$\alpha'' = -\frac{(r_2 + \varepsilon\tilde{\lambda}r_4)\tilde{K}\alpha}{\varepsilon\tilde{\lambda}r_2r_4} - \frac{\tilde{h}_1'}{r_2} - \frac{4\varepsilon\tilde{\delta}(r_2 + \varepsilon\tilde{\lambda}r_4)}{r_2r_4\tilde{\lambda}}$$
$$\times\Big\{[(1 + \varepsilon + \varepsilon\tilde{\lambda})\tilde{h}_3\cos\alpha - (r_1 + \varepsilon + \varepsilon\tilde{\lambda})\tilde{h}_2\sin\alpha]$$
$$\times\Big[(r_1 + \varepsilon + \varepsilon\tilde{\lambda} + \varepsilon^2\tilde{\delta})\tilde{h}_2\cos\alpha + (1 + \varepsilon + \varepsilon\tilde{\lambda}$$
$$+ \varepsilon^2\tilde{\delta})\tilde{h}_3\sin\alpha\Big]\Big\}\Big/\Big\{2r_1 + 2\varepsilon(1 + \tilde{\lambda})(1 + r_1) + \varepsilon^2\Big[2(1 + \tilde{\lambda})^2$$
$$+ \tilde{\delta}(1 + r_1) + (1 - r_1)\tilde{\delta}\cos 2\alpha\Big] + 2\varepsilon^3\tilde{\delta}(1 + \tilde{\lambda})\Big\}^2 \tag{22}$$

where $\tilde{h}_1'$ in Eq. (22) does not include the nonlinear controller term from Eq. (19). Equations (19–22) are the full equations of motion with no simplifying assumptions. These equations must be transformed into the aforementioned form consisting of an unperturbed part (found by discarding higher order terms; the unperturbed equations are just the equations for a torque-free rigid body) plus perturbation terms [see Eq. (16)] to apply Melnikov's method. This is done by expanding the equations in powers of ε and keeping only terms through the appropriate order of ε. The expanded equations can be written as

$$\tilde{h}_1' = \left(\frac{1 - r_1}{r_1}\right)\tilde{h}_2\tilde{h}_3 - \frac{\varepsilon(1 + \tilde{\lambda})\left(1 - r_1^2\right)}{r_1^2}\tilde{h}_2\tilde{h}_3 - \varepsilon\tilde{\beta}\tilde{h}_1\tilde{h}_2^2 + \mathcal{O}(\varepsilon^2) \tag{23}$$

$$\tilde{h}_2' = \left(\frac{r_1 - r_2}{r_1r_2}\right)\tilde{h}_1\tilde{h}_3 + \frac{\varepsilon(1 + \tilde{\lambda})\tilde{h}_1\tilde{h}_3}{r_1^2} - \frac{\varepsilon\tilde{\lambda}r_4(r_2\alpha' + \tilde{h}_1)\tilde{h}_3}{r_2^2}$$
$$+ \varepsilon\tilde{\beta}\tilde{h}_2\left(\tilde{h}_1^2 - \tilde{h}_3^2\right) + \mathcal{O}(\varepsilon^2) \tag{24}$$

$$\tilde{h}_3' = \left(\frac{r_2 - 1}{r_2}\right)\tilde{h}_1\tilde{h}_2 + \frac{\varepsilon\tilde{\lambda}r_4(\tilde{h}_1 + r_2\alpha')\tilde{h}_2}{r_2^2}$$
$$- \varepsilon(1 + \tilde{\lambda})\tilde{h}_1\tilde{h}_2 + \varepsilon\tilde{\beta}\tilde{h}_2^2\tilde{h}_3 + \mathcal{O}(\varepsilon^2) \tag{25}$$

$$\alpha'' = -(\tilde{K}/\varepsilon\tilde{\lambda}r_4)\alpha - [(1 - r_1)/r_1r_2]\tilde{h}_2\tilde{h}_3 + \mathcal{O}(\varepsilon) \qquad (26)$$

Note that the presence of ε in the denominator of the coefficient of α in Eq. (26) is a consequence of the fact that the moments of inertia of the appendage are small [see Eqs. (15) and (18)]. The effect of this term is to make the oscillatory part of the solution of Eq. (26) be high frequency. Of course, if the stiffness of the supporting shaft happens to be of order ε, then this frequency will be of order one. In addition, despite the appearance of a singularity in Eq. (26), i.e., the stiffness term is $\mathcal{O}(1/\varepsilon)$, we note that setting $\varepsilon = 0$ makes the α equation irrelevant because the terms involving α in Eqs. (23–25) disappear.

Unperturbed Phase Space

At this point we begin our discussion on how chaotic dynamics can be detected in Eqs. (10–12) and (15). First we describe the necessary phase-space structure.

The unperturbed system is obtained by discarding higher order terms in Eqs. (23–26). Note that, upon doing so, we obtain two sets of uncoupled equations

1) Equations (23–25) become Euler's equations of rotational motion.

2) Equation (26) becomes a linear oscillator forced by the angular momentum components $\tilde{h}_2$ and $\tilde{h}_3$.

To apply Melnikov's method to the system of Eqs. (23–26), there must be a heteroclinic cycle in the unperturbed phase space, and the unperturbed system must be integrable.[10] It can be shown that the attitude dynamics of a torque-free rigid body, when measured in body angular momentum components, occur on the surface of the angular momentum sphere (see Fig. 3). This sphere is also the reduced phase space corresponding to Euler's equations of motion for a torque-free rigid body. These equations are given by

$$\tilde{h}_1' = [(1 - r_1)/r_1]\tilde{h}_2\tilde{h}_3 \qquad (27)$$

$$\tilde{h}_2' = \left(\frac{r_1 - r_2}{r_1r_2}\right)\tilde{h}_1\tilde{h}_3 \qquad (28)$$

$$\tilde{h}_3' = [(r_2 - 1)/r_2]\tilde{h}_1\tilde{h}_2 \qquad (29)$$

Euler's equations are integrable in terms of Jacobi elliptic functions or hyperbolic functions, depending on the angular momentum and energy (the hyperbolic function solutions correspond to the heteroclinic cycles in Fig. 3). The phase space is a two-dimensional surface embedded in $\mathbb{R}^3$. This phase space possesses six fixed points or equilibria corresponding to positive and negative spin about each of the three principal axes of the satellite. Two of the fixed points, corresponding to spin about the intermediate principal axis, are hyperbolic fixed points or saddles. In addition, there are four heteroclinic orbits linking the hyperbolic fixed points as shown in Fig. 3. During transition of an energy-dissipating satellite from spin near the minimum moment of inertia axis to spin about the maximum moment of inertia axis, the trajectory must cross the heteroclinic orbits in the phase space. More precisely, the trajectory of the damped system must cross a heteroclinic orbit of the undamped system.

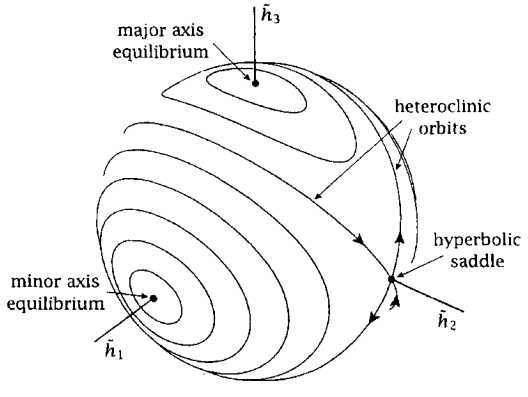

Fig. 3 Momentum sphere illustrating heteroclinic orbits and hyperbolic saddle points. Curves are orbits of constant energy.

Application of Melnikov's Method

Now that we have the requisite phase-space structure needed to apply Melnikov's method, we briefly describe the method and how we apply it. Melnikov's method is a perturbation technique that provides a measure of the distance or separation between the stable and unstable manifolds of hyperbolic saddles in planar Poincaré maps. If the manifolds intersect transversely in the Poincaré map, each intersection is referred to as a transverse heteroclinic point, and infinitely many such points must exist. (The method applies equally well to systems with homoclinic orbits.) The existence of transverse heteroclinic points in the Pioncaré map implies the existence of horseshoes and chaos via the Smale–Birkhoff theorem.[8] Melnikov's method proves the existence of transverse heteroclinic points by determining when the distance between the stable and unstable manifolds is zero for some values of the system's parameters. Although it is a perturbation technique, Melnikov's method gives global information about the system's dynamics. The essential idea is to use the globally computable solutions to the unperturbed integrable system in studying the perturbed solution. For a detailed exposition of Melnikov theory, see Guckenheimer and Holmes[8] or Wiggins.[9,10]

Melnikov's method considers systems of the form

$$\dot{\boldsymbol{x}} = \boldsymbol{f}(\boldsymbol{x}) + \varepsilon\boldsymbol{g}(\boldsymbol{x}, t), \qquad \boldsymbol{x} = \begin{Bmatrix} u \\ v \end{Bmatrix} \in \mathbb{R}^2 \qquad (30)$$

where $\boldsymbol{g}$ is periodic in t, $\boldsymbol{f}(\boldsymbol{x})$ is a Hamiltonian vector field defined on $\mathbb{R}^2$, and $\varepsilon\boldsymbol{g}(\boldsymbol{x}, t)$ is a small perturbation that is not necessarily Hamiltonian. The Melnikov function, denoted $\mathcal{M}(t_0)$, can be written as the integral

$$\mathcal{M}(t_0) = \int_{-\infty}^{\infty} \boldsymbol{f}[\boldsymbol{q}_0(t)] \wedge \boldsymbol{g}[\boldsymbol{q}_0(t), t + t_0]\, dt \qquad (31)$$

where the symbol $\wedge$ is the wedge operator, defined by $\boldsymbol{a} \wedge \boldsymbol{b} = a_1b_2 - a_2b_1$ and $\boldsymbol{q}_0(t)$ is the solution for the heteroclinic orbits in the unperturbed system.

Melnikov's method previously has been applied to simple spacecraft systems by Gray et al.,[5,6] yielding previously unknown results about the complex dynamics of perturbed rigid bodies. This study extends those results to similar spacecraft systems possessing elastic elements. Equations (23–26) must first be written in the form of Eq. (30) and the unperturbed or $\mathcal{O}(1)$ terms must be fully integrable. This is done in the following manner (following a technique of Holmes[21] and Wiggins[9]).

Step 1. We begin by noting that Eqs. (23–25) are coupled to Eq. (26) only through perturbations of the $\tilde{h}_i'$ equations. That is, the $\mathcal{O}(1)$ terms in Eqs. (23–25) do not contain α. This allows us to solve for the unperturbed orbits $\tilde{h}_i$ without regard to the α equation.

Step 2. Now that we have the solutions for the unperturbed angular momentum components $\tilde{h}_i$, we substitute those solutions into the corresponding $\tilde{h}_i$ components of α Eq. (26). We then solve the resulting equation, which is a linear oscillator forced by hyperbolic functions, for α.

Step 3. Finally, we substitute the solutions obtained in Step 2 for α (and α' by differentiation) into the perturbation terms of Eqs. (23–25). Because the solutions for α turn out to be periodic, that leaves us with three nonautonomously forced equations [forced in the $\mathcal{O}(\varepsilon)$ perturbations] in the three components of angular momentum.

We now describe each of the three steps in detail.

Step 1: unperturbed heteroclinic orbits $\boldsymbol{q}_0(t)$. We obtain the solutions to Eqs. (23–25) along the unperturbed heteroclinic orbits by discarding higher order terms, thus obtaining Euler's equation of rotational motion. For a torque-free rigid body with equations of motion given by Eqs. (27–29), there are two integrals of the motion—momentum and energy.[20] In nondimensional coordinates, these integrals are given by

$$\tilde{h}_1^2 + \tilde{h}_2^2 + \tilde{h}_3^2 = 1 \qquad \text{(momentum)} \qquad (32)$$

$$\left(\tilde{h}_1^2/r_2\right) + \tilde{h}_2^2 + \left(\tilde{h}_3^2/r_1\right) = \tilde{T} \qquad \text{(energy)} \qquad (33)$$

where $\tilde{T} \triangleq 2B_bT/h^2$ is the nondimensional total energy and T is the total energy. Any trajectory on the momentum sphere is determined by the intersection of the momentum sphere $\mathcal{S}$ defined by Eq. (32) and the energy ellipsoid $\mathcal{E}$ defined by Eq. (33). Recall that when viewed in body coordinates, the angular momentum vector appears to move so that its tip always remains on a particular intersection of $\mathcal{S}$ and $\mathcal{E}$. The radius of $\mathcal{S}$, which is $\tilde{h}=1$, must lie between the smallest and largest semiaxes of the ellipsoid. Because $A_b < B_b < C_b$, or nondimensionally $0 < r_2 < 1 < r_1$ (the complete condition on r_1 and r_2 is $0 < r_2 < 1 < r_1 < 1 + r_2$), the condition on the radius of $\mathcal{S}$ is given by $r_2\tilde{T} < 1 < r_1\tilde{T}$. Because the heteroclinic orbits are formed when the $\mathcal{S}$ and $\mathcal{E}$ surfaces are tangent at the points $(0, \pm 1, 0)$, the energy level for the heteroclinic orbits must be given by $T = h^2/(2B_b)$ or $\tilde{T}=1$ nondimensionally. The energy integral then becomes

$$\left(\tilde{h}_1^2/r_2\right) + \tilde{h}_2^2 + \left(\tilde{h}_3^2/r_1\right) = 1 \tag{34}$$

Using Eqs. (27–29), (32), and (34), it can be shown that the solutions for the $\tilde{h}_i$ along the heteroclinic orbits are given by (also see Ref. 20)

$$\tilde{h}_1 = \pm\left[\frac{r_2(1-r_1)}{r_2-r_1}\right]^{\frac{1}{2}} \operatorname{sech}[\aleph\tau] \tag{35}$$

$$\tilde{h}_2 = \pm \tanh[\aleph\tau] \tag{36}$$

$$\tilde{h}_3 = \pm\left[\frac{r_1(r_2-1)}{r_2-r_1}\right]^{\frac{1}{2}} \operatorname{sech}[\aleph\tau] \tag{37}$$

where

$$\aleph = \sqrt{\frac{(r_1-1)(1-r_2)}{(r_1r_2)}}$$

$\tau = 0$ has been chosen to eliminate constants of integration, and the appropriate signs are chosen to give the four heteroclinic trajectories. Note that these solutions, [Eqs. (35–37)] are also the unperturbed solutions to our equations of motion [Eqs. (23–25)] because when higher order terms are discarded in Eqs. (23–25), we just obtain Euler's equations of rotational motion.

Step 2: solving the α equation. The solution to the equation for α that is obtained after substituting the unperturbed solutions for $\tilde{h}_2$ and $\tilde{h}_3$ into Eq. (26) is derived in the Appendix. It is shown that the solution to Eq. (26) is

$$\begin{aligned}\alpha = &\left\{\alpha_0 - \frac{\pi}{2(1-r_2)}\operatorname{sech}\left[\frac{\pi\Omega}{2\aleph}\right]\right\}\cos[\Omega\tau] \\ &+\left\{\frac{\alpha_0'}{\Omega} + \frac{r_1-1}{\Omega\aleph r_1r_2} + \frac{\pi}{2(1-r_2)}\left(\pi\tanh\left[\frac{\pi\Omega}{2\aleph}\right]\right.\right. \\ &\left.\left.-i\psi\left[\frac{\aleph+i\Omega}{4\aleph}\right]+i\psi\left[\frac{\aleph-i\Omega}{4\aleph}\right]\right)\right\}\sin[\Omega\tau]\end{aligned} \tag{38}$$

or rather

$$\alpha = \mathcal{A}\sin(\Omega\tau + \Upsilon) \tag{39}$$

where $\mathcal{A}$ is the amplitude and Υ is the phase of Eq. (38), $\Omega \triangleq \sqrt{[\tilde{K}/(\varepsilon\tilde{\lambda}r_4)]}$, α_0 is the initial angle of twist, α_0' is the initial angle of twist rate, and ψ is the Euler psi function (also known as the Digamma function).

Step 3: substitution of α. We now incorporate the unperturbed solution for α into the $\mathcal{O}(\varepsilon)$ terms of the angular momentum Eqs. (23–25). Because of their length, the equations are not shown here, but they are carried along implicitly in the next section, where we transform to spherical coordinates. In general, this procedure would be sufficient for application of Melnikov's method. However, we need to transform the equations of motion into spherical coordinates so we will have independent equations.

Transforming the $\mathcal{O}(\varepsilon)$ to Spherical Coordinates

We now transform to spherical coordinates so that the surface of the momentum sphere is mapped to the plane. This is done because the $\tilde{h}_i'$ equations are not independent (three equations are describing the motion on a two-dimensional surface). Transforming to spherical coordinates will give us two independent equations. It is convenient to choose the coordinate transformation so that one of the new coordinates is zero along an unperturbed trajectory. This can be done easily because the heteroclinic orbits are great circles on the momentum sphere. Consider the heteroclinic orbit that lies in the region $\tilde{h}_1 > 0$ and $\tilde{h}_3 > 0$. The angle ν between the $\tilde{h}_1$–$\tilde{h}_2$ plane and this heteroclinic orbit can be shown to be

$$\nu = \arctan\sqrt{\frac{r_1(r_2-1)}{r_2(1-r_1)}} \tag{40}$$

From this definition for the angle ν, we also can show that

$$\cos\nu = \sqrt{\frac{r_2(r_1-1)}{r_1-r_2}}, \qquad \sin\nu = \sqrt{\frac{r_1(1-r_2)}{r_1-r_2}}$$

Starting with a set of coordinates ξ_1, ξ_2, ξ_3 aligned with the e_1, e_2, e_3 system, we can rotate the $\boldsymbol{\xi}$ coordinate system through the angle $-\nu$ about the $\tilde{h}_2$ axis so that the positive ξ_1 axis pierces the heteroclinic orbit in the region $\tilde{h}_1 > 0$, $\tilde{h}_3 > 0$. We can then transform from the $\boldsymbol{\xi}$ coordinates to the spherical coordinates ϕ and θ to obtain the following equations relating the $\tilde{h}_i$, ν, θ, and ϕ:

$$\tilde{h}_1 = \cos\nu\cos\theta\cos\phi - \sin\nu\sin\phi \tag{41}$$

$$\tilde{h}_2 = \sin\theta\cos\phi \tag{42}$$

$$\tilde{h}_3 = \sin\nu\cos\theta\cos\phi + \cos\nu\sin\phi \tag{43}$$

Note that there is no radial dependence because the angular momentum sphere has a constant radius. It is important to note that this transformation does not alter our Melnikov results or their interpretation. In fact, we really are just transforming a planar system (S^2—the surface of the sphere) to a planar system ($\mathbb{R}^2$). Because the transformation given in Eqs. (41–43) is a diffeomorphism (a diffeomorphism from one manifold M to another N is a one-to-one, onto, differentiable map $\Phi : M \to N$ such that the inverse $\Phi^{-1} : N \to M$ is also differentiable), points of intersection on the surface of the sphere must remain points of intersection in the plane, and if the intersection is transversal in one it must be transversal in the other. This is the natural idea of isomorphism, or sameness, for manifolds.

The derivatives with respect to τ are also needed and they are given by

$$\tilde{h}_1' = \phi'(-\cos\nu\sin\phi\cos\theta - \sin\nu\cos\phi) - \theta'\cos\nu\sin\theta\cos\phi \tag{44}$$

$$\tilde{h}_2' = \theta'\cos\theta\cos\phi - \phi'\sin\theta\sin\phi \tag{45}$$

$$\tilde{h}_3' = \phi'(\cos\nu\cos\phi - \sin\nu\cos\theta\sin\phi) - \theta'\sin\nu\sin\theta\cos\phi \tag{46}$$

The unperturbed solutions given by Eqs. (35–37) must be transformed to the same set of spherical coordinates. This transformation gives

$$\sin\theta = -\tanh[\aleph\tau] \tag{47}$$

$$\cos\theta = \operatorname{sech}[\aleph\tau] \tag{48}$$

$$\phi = 0 \tag{49}$$

along the selected unperturbed heteroclinic orbit, with time chosen to move along the trajectory from positive to negative $\tilde{h}_2$.

Substituting Eqs. (41–46) into Eqs. (23–25) and then solving any two of the resulting three equations for θ' and ϕ' gives the final

two first-order differential equations to which Melnikov's method is applied:

$$\theta' \triangleq f_\theta + \varepsilon g_\theta \tag{50}$$

$$\phi' \triangleq f_\phi + \varepsilon g_\phi \tag{51}$$

where $\{f_\theta, f_\phi\} = f$ and $\{g_\theta, g_\phi\} = g$ [see Eq. (30)].

Melnikov Function

Substituting the unperturbed solutions $q_0(\tau)$, given by Eqs. (47–49), into $f[q_0(\tau)]$ and $g[q_0(\tau), \tau + \tau_0]$ [defined in Eqs. (50) and (51)], carrying out the wedge product, substituting the result into the Melnikov integral given by Eq. (31), and eliminating terms that are zero because of having an odd integrand, we obtain

$$\mathcal{M}(\tau_0) = -c_7 r_2 \aleph \Omega \mathcal{A} \cos\nu \int_{-\infty}^{\infty} \operatorname{sech}(\aleph\tau)\tanh(\aleph\tau) \times \cos[\Omega(\tau+\tau_0)+\Upsilon]\,d\tau - \tilde{\beta}\aleph \sin 2\nu \int_{-\infty}^{\infty} \operatorname{sech}^2(\aleph\tau)\tanh^2(\aleph\tau)\,d\tau \tag{52}$$

where $c_7 \triangleq -\tilde{\lambda} r_4 / r_2^2$.

The evaluation of these integrals can be determined with integration by parts and a good set of integral tables.[22] After integrating, the following Melnikov function is obtained:

$$\mathcal{M}(\tau_0) = -\frac{2\tilde{\beta}}{3}\sin 2\nu - \frac{\pi \tilde{K}\mathcal{A}\cos\nu}{\varepsilon r_2 \aleph \cosh[\pi\Omega/(2\aleph)]}\sin(\Omega\tau_0 + \Upsilon) \tag{53}$$

Melnikov theory states that the condition for chaos is that $\mathcal{M}(\tau_0)$ change sign for some τ_0. Inspection of the Melnikov function reveals that the condition for chaos is

$$3\pi\tilde{K}\mathcal{A} > 4\varepsilon\tilde{\beta}\aleph r_2 \sin\nu \cosh(\pi\Omega/2\aleph) \tag{54}$$

That is, if Eq. (54) is satisfied, then the system exhibits chaotic dynamics near the heteroclinic orbits for sufficiently small ε.

Interpretation of the Melnikov Criterion

We have analytically proven the existence of horseshoes in the attitude motion of a satellite perturbed by both continuous elastic elements and an energy-dissipating nonlinear controller. The derived criterion can be used to find the hypersurface separating chaotic and nonchaotic regions in parameter space and, if necessary, to avoid chaotic motion in this class of spacecraft systems. Inspection of Eq. (54) reveals that the Melnikov criterion is a function of the seven system parameters ($r_1, r_2, r_4, \varepsilon, \tilde{\lambda}, \tilde{K}$, and $\tilde{\beta}$). If we satisfy Eq. (54), the previously mentioned restriction on the carrier body's shape parameters r_1 and r_2 ($0 < r_2 < 1 < r_1 < 1 + r_2$), and the restrictions on the control gain (damping parameter) $\tilde{\beta}$ given by Eq. (13), then the system, modeled by Eqs. (10–12) and (15), exhibits chaotic dynamics near the unperturbed heteroclinic orbits for sufficiently small ε.

Investigation of the implications of the criterion for chaos given in Eq. (54) can be done by fixing four of the seven system parameters and then studying the others in a three-dimensional parameter subspace. Parametric studies of three-dimensional parameter subspaces for Eq. (54) are shown in Figs. 4–8, where the chaotic parameter region is above the surface. We note here that Figs. 4–8 were determined by using Eq. (13) as well as the Melnikov criterion [Eq. (54)], i.e., when the value of $\tilde{\beta}$ required to avoid chaos exceeds the value allowed by Eq. (13), we show this with a flat surface at that level, thus indicating that the values of $\tilde{\beta}$ necessary to avoid chaos cannot be achieved for the set of parameter values corresponding to the flat surface. These investigations will eventually need to be compared with numerical experiments, but the numerical experiments have turned out to be too numerous and extensive to be presented here and will be presented in another paper.

One characteristic that is immediately obvious is that as the control gain $\tilde{\beta}$ is increased, it becomes increasingly more difficult to satisfy the Melnikov criterion [Eq. (54)] or, rather, achieve chaotic motion. It can also be seen that as $\tilde{\beta} \to 0$, chaotic motion occurs for all values of the system parameters, which is to be expected from the theory of Hamiltonian systems; a generic Hamiltonian perturbation to a Hamiltonian system always yields chaotic motion in a layer surrounding a separatrix.[23]

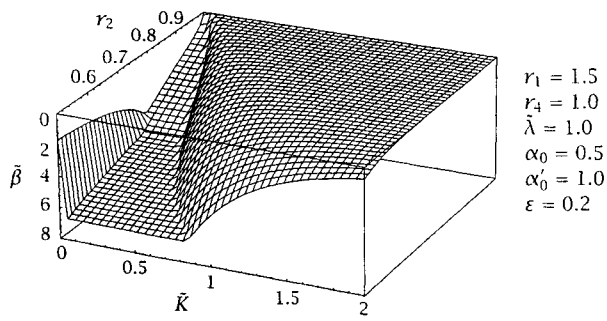

Fig. 4 Surface separating chaotic from nonchaotic motion in $\tilde{K}, r_2, \tilde{\beta}$ space showing that for a nearly symmetric oblate carrier body, chaos is very difficult to achieve.

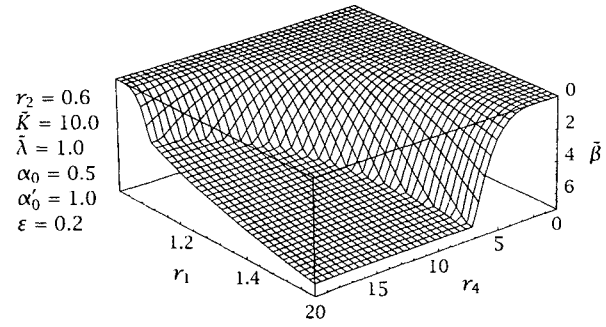

Fig. 5 Surface separating chaotic from nonchaotic motion in $r_1, r_4, \tilde{\beta}$ space showing that for a nearly symmetric prolate carrier body, chaos is very difficult to achieve.

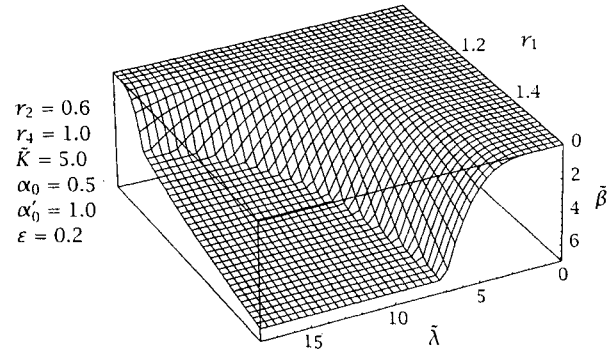

Fig. 6 Surface separating chaotic from nonchaotic motion in $r_1, \tilde{\lambda}, \tilde{\beta}$ space showing the influence of appendage size on chaotic dynamics.

In Fig. 4, we see that as the carrier body becomes a nearly symmetric oblate body ($r_2 \to 1$), we have that the minimum value of control gain $\tilde{\beta}$ needed to avoid chaos approaches zero, that is, chaos is very difficult to achieve. (Recall that a prolate body is one shaped like a rod or thin cylinder and an oblate body is shaped like a coin or a squat cylinder.[24] Also recall that $C_b > B_b > A_b$ and that $r_2 \triangleq A_b/B_b$ and therefore as $r_2 \to 1$, A_b and B_b approach one another and the satellite becomes an oblate-like body. As C_b and B_b approach one another, i.e., $r_1 \to 1$, the satellite becomes a prolate-like body. Note that one of the underlying assumptions in all this work is that $A_b \neq B_b \neq C_b$, implying an asymmetric body. Without this, application of Melnikov's method is impossible. Therefore, when the statement $r_2 \to 1$ is made, we are not saying that the body becomes symmetric with $A_b = B_b$ but that the body becomes nearly symmetric.) As r_2 approaches the opposite limit of the carrier body's shape inequality ($r_2 \to r_1 - 1$), the minimum value of $\tilde{\beta}$ needed to avoid chaos increases in magnitude. In Figs. 5 and 6, we see that as the carrier body becomes a nearly

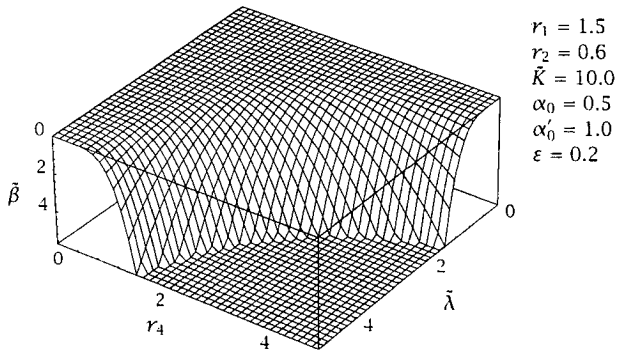

Fig. 7 Surface separating chaotic from nonchaotic motion in r_4, $\tilde{\lambda}$, $\tilde{\beta}$ space showing the influence of appendage shape on chaotic dynamics.

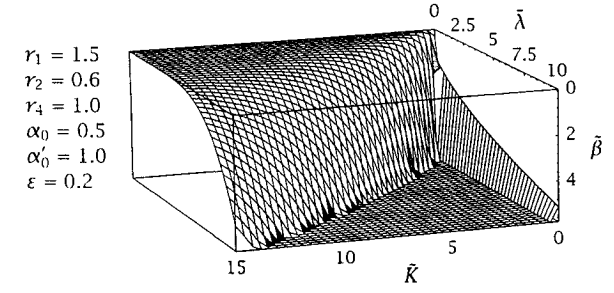

Fig. 8 Surface separating chaotic from nonchaotic motion in $\tilde{K}$, $\tilde{\lambda}$, $\tilde{\beta}$ space showing the influence of appendage stiffness on chaotic dynamics.

symmetric prolate body ($r_1 \to 1$), the minimum value of $\tilde{\beta}$ needed to avoid chaos approaches zero. As r_1 approaches the opposite limit of the carrier body's shape inequality ($r_1 \to 1 + r_2$) the minimum value of $\tilde{\beta}$ needed to avoid chaos increases in magnitude. Therefore, for the two limiting shapes represented by nearly symmetric oblate and prolate carrier bodies, chaos is very difficult to achieve. In Figs. 6–8 we see that as the appendage becomes much smaller than the carrier body ($\tilde{\lambda} \to 0$), the minimum value of $\tilde{\beta}$ needed to avoid chaos approaches zero. As $\tilde{\lambda}$ increases in magnitude, that is, as the size of the appendage relative to the size of the carrier body increases in magnitude, the minimum value of $\tilde{\beta}$ needed to avoid chaos increases in magnitude, as expected. In Figs. 5 and 7, we see that as the appendage becomes much longer along the ζ_1 axis than either the ζ_2 or ζ_3 axes ($r_4 \to 0$), the minimum value of $\tilde{\beta}$ needed to avoid chaos approaches zero. Note that the shape of the appendage depends strongly on whether r_4 is greater than or less than one. If $r_4 < 1$ the major axis of the appendage is aligned with either the ζ_2 or the ζ_3 axis when the appendage is in its undeformed state. When $r_4 > 1$, the appendage is aligned so that the major axis lies along the ζ_1 axis. As Figs. 5 and 7 show, the nature of the dynamics does not necessarily change as we pass from $r_4 < 1$ to $r_4 > 1$. However, as r_4 increases in magnitude, the minimum value of $\tilde{\beta}$ needed to avoid chaos increases in magnitude.

In Fig. 8, we see that as we decrease the torsional stiffness of the rod ($\tilde{K}$), the minimum value of $\tilde{\beta}$ needed to avoid chaos increases until $\tilde{K}$ becomes very small; for very small $\tilde{K}$, i.e., as $\tilde{K}$ approaches zero, the minimum value of $\tilde{\beta}$ needed to avoid chaos decreases sharply in magnitude. Other parameter subspaces were also studied, with similar results.

Conclusions

We have derived an analytical criterion for the occurrence of a chaotic region of phase space in terms of system parameters for a spacecraft with a nearly symmetric flexible appendage; a process that involves applying Melnikov's method to a perturbed satellite model and performing the nontrivial calculations required to obtain a criterion for chaos that can easily be used for satellite design. It may be obvious from the modern theory of dynamical systems that chaos can occur via the breakup of heteroclinic orbits in this class of systems, but we have been able to analytically predict for which parameter values this will occur for a physically realistic model. It is important to note that we have studied chaotic dynamics in a spacecraft system with energy dissipation that does not possess nonautonomous forcing terms. In other words, the chaos comes from the vibration of continuous elastic elements on the spacecraft and not from some nonautonomous periodic forcing function such as a misaligned rotor. Thus we have shown that even a perfectly tuned spacecraft system, with a control system designed to provide energy dissipation, can exhibit chaos as a result of the inherent flexibility of its components. The analytic criterion in this paper thus gives a useful design tool to spacecraft engineers concerned with avoiding potentially problematic chaotic dynamics in their systems.

Appendix: Solution for α

We present here the derivation of the exact solution and approximate solution to the equation of the form

$$\ddot{\alpha} + \omega^2 \alpha = F \tag{A1}$$

where $F = A\,\mathrm{sech}(bt)\tanh(bt)$.

Following a standard variation of parameters procedure, we have that the solution to Eq. (A1) is

$$\alpha = u_1 v_1 + u_2 v_2 \tag{A2}$$

where $D = \omega$ and

$$u_1 = \cos\omega t, \qquad \dot{v}_1 = -\frac{u_2 F}{D}, \qquad v_1(t) = v_1(0) + \int_0^t \dot{v}_1\,\mathrm{d}t$$

$$u_2 = \sin\omega t, \qquad \dot{v}_2 = \frac{u_1 F}{D}, \qquad v_2(t) = v_2(0) + \int_0^t \dot{v}_2\,\mathrm{d}t$$

To find expressions for $v_1(0)$ and $v_2(0)$, we first evaluate α and $\dot{\alpha}$ at $t = 0$

$$\alpha(0) = u_1(0)\,v_1(0) + u_2(0)\,v_2(0) = v_1(0)$$

$$\dot{\alpha}(0) = \dot{u}_1(0)\,v_1(0) + u_1(0)\,\dot{v}_1(0) + \dot{u}_2(0)\,v_2(0) + u_2(0)\,\dot{v}_2(0) = v_2(0)\omega$$

Then $\alpha(0) = \alpha_0 \Rightarrow v_1(0) = \alpha_0$, and $\dot{\alpha}(0) = \dot{\alpha}_0 \Rightarrow v_2(0) = \dot{\alpha}_0/\omega$. So, our solution to Eq. (A1) can be written as

$$\alpha(t) = \left[\alpha_0 + \int_0^t \dot{v}_1\,\mathrm{d}t\right]\cos\omega t + \left[\frac{\dot{\alpha}_0}{\omega} + \int_0^t \dot{v}_2\,\mathrm{d}t\right]\sin\omega t \tag{A3}$$

Note that $\dot{v}_1$ and $\dot{v}_2$ do not have elementary antiderivatives. However, because $\dot{v}_1$ and $\dot{v}_2$ decay to zero as t becomes large, we have the following approximation to Eq. (A3):

$$\alpha(t) \approx \bar{\alpha}(t) = \bar{C}_1 \cos\omega t + \bar{C}_2 \sin\omega t \tag{A4}$$

where

$$\bar{C}_1 = \alpha_0 + \int_0^\infty \dot{v}_1\,\mathrm{d}t, \qquad \bar{C}_2 = \frac{\dot{\alpha}_0}{\omega} + \int_0^\infty \dot{v}_2\,\mathrm{d}t$$

As we shall see, closed-form expressions do exist for the integrals found in the preceding expressions for $\bar{C}_1$ and $\bar{C}_2$. Integrating by parts, we obtain

$$\int_0^\infty \dot{v}_1\,\mathrm{d}t = -\int_0^\infty \frac{\sin\omega t\,(A\,\mathrm{sech}\,bt\tanh bt)}{\omega}\,\mathrm{d}t$$

$$= \frac{-A}{b}\int_0^\infty \frac{\cos\omega t}{\cosh bt}\,\mathrm{d}t \tag{A5}$$

and from formula 3.981.3 of Ref. 22, we have that

$$\int_0^\infty \frac{\cos\omega t}{\cosh bt}\,\mathrm{d}t = \frac{\pi}{2b}\,\mathrm{sech}\left(\frac{\pi\omega}{2b}\right) \tag{A6}$$

Therefore, we obtain

$$\int_0^\infty \dot{v}_1\,dt = \frac{-A\pi}{2b^2}\,\mathrm{sech}\left(\frac{\pi\omega}{2b}\right) \tag{A7}$$

Similarly, integrating by parts and using formula 3.981.2 of Ref. 22 we obtain

$$\int_0^\infty \dot{v}_2\,dt = \int_0^\infty \frac{\cos\omega t\,(A\,\mathrm{sech}\,bt\tanh bt)}{\omega}\,dt \tag{A8}$$

$$= \frac{A}{\omega}\left\{\frac{1}{b} - \frac{\omega}{b}\int_0^\infty \frac{\sin\omega t}{\cosh bt}\,dt\right\} \tag{A9}$$

$$= \frac{A}{b\omega}\left(1 + \frac{\omega}{2b}\left\{\pi\tanh\left(\frac{\pi\omega}{2b}\right) + i\left[\psi\left(\frac{b+i\omega}{4b}\right) - \psi\left(\frac{b-i\omega}{4b}\right)\right]\right\}\right) \tag{A10}$$

where ψ, the Euler psi or Digamma function, is defined as

$$\psi(z) = \int_0^\infty \left\{e^{-\tau} - \frac{1}{(1+\tau)^z}\right\}\frac{d\tau}{\tau} \qquad \Re(z) > 0 \tag{A11}$$

$$|\alpha(t) - \bar{\alpha}(T_N)| = \left|\cos\omega t\int_{T_N}^\infty \dot{v}_1\,dt + \sin\omega t\int_{T_N}^\infty \dot{v}_2\,dt\right|$$

$$\le \left|\cos\omega t\int_{T_N}^\infty \dot{v}_1\,dt\right| + \left|\sin\omega t\int_{T_N}^\infty \dot{v}_2\,dt\right|$$

$$\le |\cos\omega t|\left|\int_{T_N}^\infty \dot{v}_1\,dt\right| + |\sin\omega t|\left|\int_{T_N}^\infty \dot{v}_2\,dt\right|$$

$$\le \left|\int_{T_N}^\infty \dot{v}_1\,dt\right| + \left|\int_{T_N}^\infty \dot{v}_2\,dt\right|$$

$$\le \int_{T_N}^\infty |\dot{v}_1|\,dt + \int_{T_N}^\infty |\dot{v}_2|\,dt$$

$$\le \int_{T_N}^\infty \left|\frac{-A}{\omega}\sin\omega t\,(\mathrm{sech}\,bt\tanh bt)\right|dt$$

$$+ \int_{T_N}^\infty \left|\frac{A}{\omega}\cos\omega t\,(\mathrm{sech}\,bt\tanh bt)\right|dt$$

$$\le \int_{T_N}^\infty |\sin\omega t|\left|\frac{-A}{\omega}\mathrm{sech}\,bt\tanh bt\right|dt$$

$$+ \int_{T_N}^\infty |\cos\omega t|\left|\frac{A}{\omega}\mathrm{sech}\,bt\tanh bt\right|dt$$

Finally, we have that

$$|\alpha(t) - \bar{\alpha}(T_N)| \le \frac{2|A|}{\omega}\int_{T_N}^\infty \mathrm{sech}\,bt\tanh bt\,dt$$

$$\le \frac{2|A|\,\mathrm{sech}\,bT_N}{b\omega}$$

So, given values for A, b, and k, we can choose T_N so that the error between the exact and approximate solutions will be as small as we like for all values of t greater than T_N.

References

[1]Mazzoleni, A. P., and Schlack, A. L., "Full Field Stability Analysis of Guy-Wired Satellites," *Journal of Astronautical Sciences*, Vol. 43, No. 1, 1995, pp. 47–58.

[2]Mazzoleni, A. P., Hall, C. D., and Stabb, M. C., "Double Averaging Approach to the Study of Spinup Dynamics of Flexible Satellites," *Journal of Guidance, Control, and Dynamics*, Vol. 19, No. 1, 1996, pp. 54–59.

[3]Stabb, M. C., and Schlack, A. L., "Pointing Accuracy of a Dual-Spin Satellite due to Torsional Appendage Vibrations," *Journal of Guidance, Control, and Dynamics*, Vol. 16, No. 4, 1993, pp. 630–635.

[4]Kammer, D. C., and Gray, G. L., "A Nonlinear Control Design for Energy Sink Simulation in the Euler–Poinsot Problem," *Journal of Astronautical Sciences*, Vol. 41, No. 1, 1993, pp. 53–72.

[5]Gray, G. L., Kammer, D. C., and Dobson, I., "Detection of Chaotic Saddles in an Attitude Maneuver of a Spacecraft Containing a Viscous Damper," Proceedings of the AAS/AIAA Spaceflight Mechanics Meeting (Pasadena, CA), *Advances in the Astronautical Sciences*, Vol. 82, Feb. 1993, pp. 167–184 (AAS Paper 93-133).

[6]Gray, G. L., Dobson, I., and Kammer, D. C., "Chaos in a Spacecraft Attitude Manuever Due to Time-Periodic Perturbations," *Journal of Applied Mechanics*, Vol. 63, No. 2, 1996, pp. 501–508.

[7]Gray, G. L., and Campbell, D. R., III, "Numerical Investigation of Complex Dynamics and Chaos in a Satellite Attitude Maneuver," Thirty-Second Annual Technical Meeting of the Society of Engineering Science (New Orleans, LA), Oct.–Nov. 1995.

[8]Guckenheimer, J., and Holmes, P., *Nonlinear Oscillations, Dynamical Systems, and Bifurcations of Vector Fields*, Springer–Verlag, New York, 1983.

[9]Wiggins, S., *Global Bifurcations and Chaos*, Springer–Verlag, New York, 1988.

[10]Wiggins, S., *Introduction to Applied Nonlinear Dynamical Systems and Chaos*, Springer–Verlag, New York, 1990.

[11]Abraham, R., and Marsden, J. E., *Foundations of Mechanics*, 2nd ed., Benjamin/Cummings, Reading, MA, 1978.

[12]Holmes, P. J., and Marsden, J. E., "Horseshoes and Arnold Diffusion for Hamiltonian Systems on Lie Groups," *Indiana University Mathematics Journal*, Vol. 32, No. 2, 1983, pp. 273–309.

[13]Koiller, J., "A Mechanical System with a 'Wild' Horseshoe," *Journal of Mathematical Physics*, Vol. 25, No. 5, 1984, pp. 1599–1604.

[14]Chernous'ko, F. L., "On the Motion of a Solid Body with Elastic and Dissipative Elements," *Applied Mathematics and Mechanics*, Vol. 42, No. 1, 1978, pp. 32–41.

[15]Chernous'ko, F. L., and Shamaev, A. S., "Asymptotic Behavior of Singular Perturbations in the Problem of Dynamics of a Rigid Body with Elastic and Dissipative Elements," *Mechanics of Solids*, Vol. 18, No. 3, 1983, pp. 31–41.

[16]Kaplan, M. H., and Beck, N. M., Jr., "Attitude Dynamics and Control of an Apogee Motor Assembly with Paired Satellites," *Journal of Spacecraft and Rockets*, Vol. 9, No. 6, 1972, pp. 410–415.

[17]Kaplan, M. H., and Cenker, R. J., "Control of Spin Ambiguity During Reorientation of an Energy Dissipating Body," *Journal of Spacecraft and Rockets*, Vol. 10, No. 12, 1973, pp. 757–760.

[18]Modi, V. J., "Attitude Dynamics of Satellites with Flexible Appendages—A Brief Review," *Journal of Spacecraft and Rockets*, Vol. 11, No. 11, 1974, pp. 743–751.

[19]Modi, V. J., "Spacecraft Attitude Dynamics: Evolution and Current Challenges," *Acta Astronautica*, Vol. 21, No. 10, 1990, pp. 689–718.

[20]Hughes, P. C., *Spacecraft Attitude Dynamics*, Wiley, New York, 1986.

[21]Holmes, P. J., "Bifurcation and Chaos in a Simple Feedback Control System," *Twenty-Second IEEE Conference on Decision and Control*, Vol. 1, Inst. of Electrical and Electronics Engineers, New York, 1983, pp. 365–370.

[22]Gradshteyn, I. S., and Ryzhik, I. M., *Table of Integrals, Series, and Products: Corrected and Enlarged Edition*, Academic, New York, 1983.

[23]Lichtenberg, A. J., and Lieberman, M. A., *Regular and Chaotic Dynamics*, 2nd ed., Springer–Verlag, New York, 1992.

[24]Wiesel, W. E., *Spaceflight Dynamics*, McGraw–Hill, New York, 1989.